Reprinted from MONTHLY WEATHER REVIEW, Vol. 118, No. 3, March 1990
American Meteorological Society

Tropical Cyclone Simulations with the Betts Convective Adjustment Scheme. Part II: Sensitivity Experiments

JONG-JIN BAIK

Department of Marine, Earth, and Atmospheric Sciences, North Carolina State University, Raleigh, North Carolina

MARK DEMARIA

Hurricane Research Division, AOML/NOAA, Miami, Florida

SETHU RAMAN

Department of Marine, Earth, and Atmospheric Sciences, North Carolina State University, Raleigh, North Carolina

(Manuscript received 10 March 1989, in final form 2 August 1989)

ABSTRACT

Extensive sensitivity experiments with an axisymmetric tropical cyclone model that includes the Betts convective parameterization scheme are carried out. The sensitivity of the model storm evolution to the convective adjustment parameters is studied. These results show that the model storm leads to earlier development as the adjustment time scale becomes small and the stability weight on the moist adiabat in the lower atmosphere is increased. The model storm evolution is very sensitive to variations in the saturation pressure departure at the lowermost model integer level and the storm at mature stage has a lower central pressure as the magnitude of the saturation pressure departure is increased. The adjustment parameters affect the grid-scale precipitation as well as the convective precipitation and the precipitation is especially sensitive to changes in the saturation pressure departure.

Sensitivity of the model to variations in the sea surface temperature, latitude, initial vortex amplitude, initial moisture distribution, and radiation is also investigated. The results of the numerical simulations are similar to previous studies. Sensitivity studies with various horizontal resolutions show that the subgrid-scale heating becomes a larger fraction of the total heating as the horizontal grid size is increased.

1. Introduction

In the tropics, a surface air parcel lifted through a pseudoadiabatic process, in which all the condensed water (or ice) is assumed to fall as precipitation immediately after it forms, is usually warmer than the environment. In this respect, the tropical atmosphere is unstable to the boundary layer convection. However, a parcel lifted in such a way that it undergoes a reversible process (where the condensed water does not fall out) has a buoyancy reduction due to the weight of the condensate. Accordingly, the tropical atmosphere is less unstable or nearly neutral (Rotunno and Emanuel 1987) to the boundary layer convection. Other buoyancy reducing effects such as entrainment, friction, compensating downward motion by the environment etc. should also be taken into account to explain the less unstable or nearly neutral state. The convective adjustment scheme proposed by Betts (1986) adjusts the local thermodynamic structures toward a quasi-equilibrium reference state where the reference state is based on observations. For example, a moist virtual adiabat, which includes the buoyancy correction due to condensed water, is used to construct the reference profile below the freezing level for deep convection and separate reference profiles are used for deep and shallow convection. The use of reference profiles based on observations should result in more realistic heating and moistening in the vertical due to cumulus convection.

In Part I (Baik et al. 1990), the convective adjustment scheme proposed by Betts (1986) was incorporated into an axisymmetric tropical cyclone model. Results showed that the convective adjustment scheme is capable of simulating the developing, rapidly intensifying, and mature stages of a tropical cyclone starting from a weak vortex. The concerns in this paper (Part II) are to study how the model storm evolution is influenced by variations in the convective adjustment parameters, physical environment, initial conditions, and horizontal resolution.

In section 2, the model is briefly summarized and in section 3, the sensitivity of the model storm evolution to the convective adjustment parameters is inves-

Corresponding author address: Dr. Sethu Raman, Dept. of Marine, Earth, and Atmospheric Sciences, North Carolina State University, Raleigh, NC 27695-8208.

tigated. In section 4, we examine the model storm sensitivity to the physical environment, initial conditions, and horizontal resolution.

2. Model summary

As described in Part I, the numerical model is an axisymmetric, primitive equation, hydrostatic, finite difference model with 15 vertical levels and a horizontal resolution of 20 km. The horizontal domain covers 1000 km and a spectral radiation condition (which uses a different gravity wave speed for each vertical mode) is applied at the outer boundary. The model includes subgrid-scale horizontal and vertical diffusion, bulk aerodynamic calculations of surface momentum, heat, and water vapor fluxes, simple radiation, grid-scale phase change, dry convective adjustment, and the Betts (1986) convective adjustment scheme for subgrid-scale moist convective processes.

The convective adjustment scheme is applied adding F_T and F_q terms given by

$$F_T = \frac{T_{\text{ref}} - \bar{T}}{\tau}, \tag{2.1}$$

$$F_q = \frac{q_{\text{ref}} - \bar{q}}{\tau}, \tag{2.2}$$

to the thermodynamic and water vapor continuity equations, respectively. In (2.1) and (2.2), T is the temperature, q the water vapor mixing ratio, and τ the adjustment time scale. The subscript ref denotes the reference state and the overbar the grid point value before convection.

The adjustment or relaxation time scale was introduced to simulate the lag between the changing large-scale field and the convective response towards a quasi-equilibrium thermodynamic reference state (Betts 1986). When τ is small, the model atmosphere is adjusted quickly toward a specified thermodynamic structure. On the other hand, with a large value of τ the atmosphere moves in the direction of the large-scale forcing (Betts and Miller 1986). The numerical experiment in which the convective parameterization was excluded (Fig. 10 in Part I) is mathematically equivalent to one in which the relaxation time scale goes to infinity.

The reference profiles of T and q depend on the cloud top. Cloud base is assumed equal to the second lowest model integer level (about 960 mb for a surface pressure of 1009 mb). Cloud top is determined by lifting a parcel from the lowest model integer level (about 990 mb for a surface pressure of 1009 mb) to saturation and then along a moist adiabat to the model top. If the parcel is not buoyant at level 13, the F_T and F_q terms are set to zero. For parcels which are buoyant at level 13, the cloud top is the last level before the parcel first loses buoyancy. If cloud top is above (below) the fifth lowest model integer level (about 800 mb for a surface pressure of 1009 mb), then deep (shallow) convective reference profiles are constructed.

The reference temperature profile below the freezing level for deep convection is constructed by assuming that the slope of the reference profile is a factor w (stability weight on the moist adiabat) times that of a moist adiabat. When w equals one, the reference temperature profile is nearly moist adiabatic. As the stability weight w decreases below one, the reference temperature stratification is more unstable than that of a moist adiabat. From the freezing level to cloud top, the thermal structure linearly approaches that of the environment (model).

The reference moisture profile is determined by specifying the saturation pressure departure at the lowest model integer level (S_d). The saturation pressure departure is a measure of how far an air parcel must be vertically displaced to become saturated, so it is a

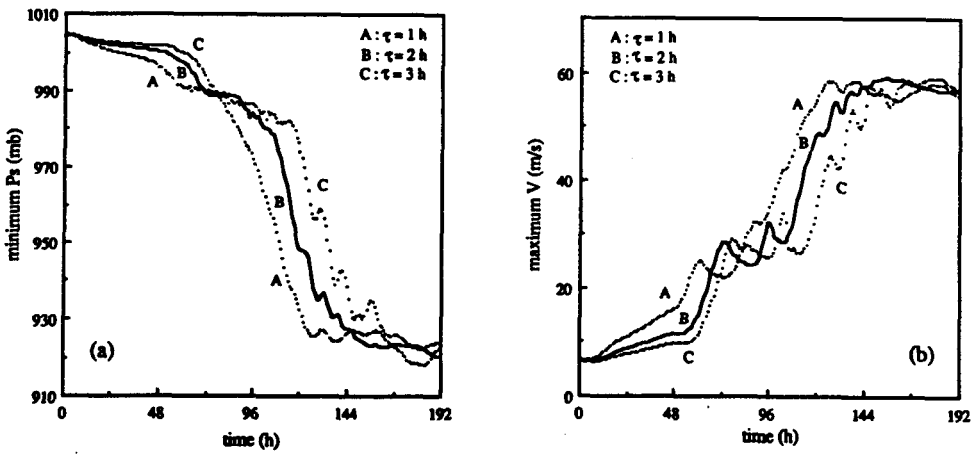

FIG. 1. (a) The time evolution of the minimum surface pressure, and (b) the maximum low level tangential wind speed for the sensitivity experiments with different adjustment time scales.

measure of relative humidity. Negative values of saturation pressure departures indicate unsaturated air. The saturation pressure departure is assumed to linearly increase (in magnitude) to a value of $1.25S_a$ at the freezing level and then linearly decrease to $0.75S_a$ at cloud top.

The reference temperature and moisture profiles for shallow convection are based on the observation that in shallow convective regions the thermodynamic structure is close to that along a mixing line that connects the saturation point of air above the cloud layer and that of the subcloud air. The shallow convective profiles are constructed in such a way that the vertically integrated heating and moistening are zero and there is no convective precipitation.

In section 3, the sensitivity of the model to the adjustment time scale τ, the stability weight w, and the saturation pressure departure S_a will be discussed. The parameter τ affects both the shallow and deep convection while w and S_a only affect the deep convection.

In Part I, results from a control simulation were presented with $\tau = 2$ hours, $w = 0.95$, and $S_a = -30$ mb. The control simulation was initialized with a cyclonic vortex in gradient wind balance with a maximum tangential wind of 7 m s^{-1} at a radius of 210 km. The initial basic temperature structure was obtained from the mean tropical clear soundings from the western Pacific and the initial moisture distribution was from the mean tropical cluster environment in the western Pacific. A Gaussian type perturbation with an amplitude of 10% and e-folding radius of 200 km was added to the initial relative humidity. The sea surface temperature was set to 28°C and the Coriolis parameter was evaluated at 20°N. The storm in the control simulation intensified slowly for about 4 days, intensified rapidly for the next 2 days, and then reached an approximate steady state. The minimum surface pressure and maximum low level tangential wind speed for the control simulation are shown in Fig. 1 (the curves labeled B).

3. Sensitivity to the convective adjustment parameters

In this section, the sensitivity of the model storm evolution to the adjustment time scale, the stability weight on the moist adiabat, and the saturation pressure departure is examined. For the sensitivity studies, each value is changed with the other two held fixed.

a. Adjustment time scale

Figure 1 shows the time histories of the minimum surface pressure and maximum low level tangential wind speed for $\tau = 1$, 2 and 3 h. This figure shows that the model storm develops earlier as the relaxation time scale becomes small. The time series with $\tau = 1$ h are slightly smoother than those with $\tau = 3$ h. In the extreme case as τ approaches infinity (Fig. 10 in Part I),

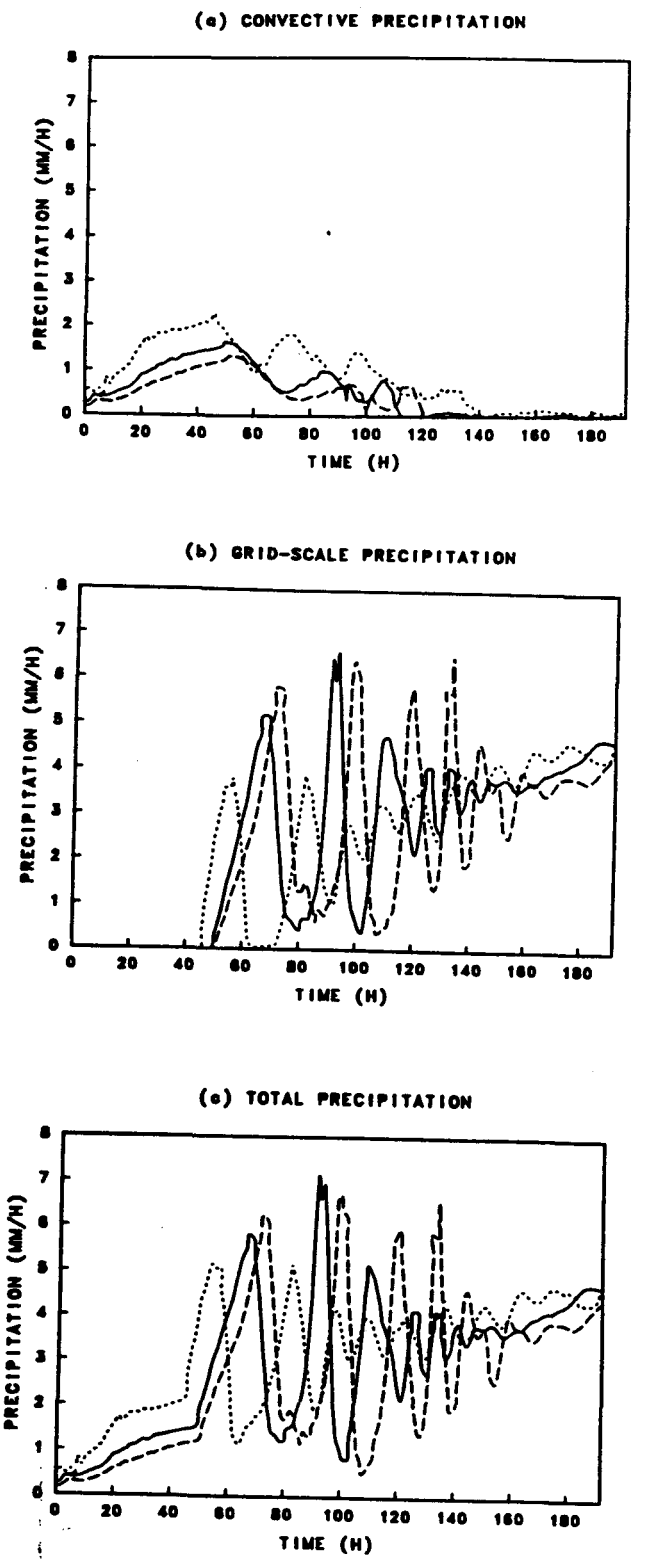

FIG. 2. (a) The time evolution of the inner 500 km domain-averaged convective, (b) grid-scale, and (c) total precipitation rates for the sensitivity experiments with different adjustment time scales. The dotted, solid, and dashed lines correspond to $\tau = 1$, 2 and 3 h, respectively.

small oscillations were also noticeable in the time evolution of the maximum low level tangential wind speed.

In order to determine the effect of the adjustment time scale on the precipitation, the time evolution of the inner 500 km domain-averaged convective, grid-scale, and total precipitation rates for τ = 1, 2 and 3 h is presented in Fig. 2. In all three simulations, only convective precipitation is present approximately during the first 2 days and then convective and grid-scale precipitations are coexistent. At the mature stages, the grid-scale precipitation is predominant. Figures 2a and 2b show that reducing τ increases the convective precipitation and decreases the grid-scale precipitation. In addition, the peaks in the convective and grid-scale precipitation occur earlier in time as τ is reduced. Betts and Miller (1986) also reported that the phase in the convective precipitation is shifted as τ is varied. Figure 2b also shows that the large amplitude oscillation in the grid-scale precipitation rate persists for a longer time period as τ is increased.

b. *Stability weight on the moist adiabat*

The time histories of the minimum surface pressure and maximum low level tangential wind speed for w = 0.90, 0.95 and 1.00 are shown in Fig. 3. This figure shows that the storm intensification occurs earlier in time as the stability weight on the moist adiabat is increased. However, the intensification rates during the rapid development period and the final intensities are similar for the three model storms.

Figure 4 shows the time evolution of the inner 500 km domain-averaged convective, grid-scale, and total precipitation rates. Compared with Fig. 2a, the convective precipitation rates do not show significant differences for the three model storms with w = 0.90, 0.95 and 1.00. The grid-scale precipitation starts at 33 h in the simulation with w = 1.00, while it begins at 50 and 57 h in the cases with w = 0.95 and 0.90, respectively. During the period from 50 to 120 h, the amplitudes in the oscillation of the grid-scale precipitation are small in the storm with w = 1.00 compared with the other two storms.

c. *Saturation pressure departure*

Figure 5 shows the time histories of the minimum surface pressure and maximum low level tangential wind speed for S_a = −20, −30 and −40 mb. The case of S_a = −20 mb gives saturation pressure departure values of −25 and −15 mb at freezing and cloud top levels, while the case of S_a = −40 mb yields the values of −50 and −30 mb. An auxiliary figure with S_a = −40 mb is shown in Fig. 6, because the 8-day time integration was not enough to obtain a mature model storm for this case. These figures indicate that the development of the model storms is very sensitive to variations in S_a. The storm with S_a = −20 mb shows large amplitude oscillations in the minimum surface pressure and maximum low level tangential wind speed. After 110 h, peak values in maximum low level tangential wind speed and corresponding peak values in minimum surface pressure occur about every 15 h. The storm with S_a = −40 mb takes a longer time period to develop compared with the other two storms, but eventually becomes more intense than the other two cases.

Figure 7 shows the time evolution of the inner 500 km domain-averaged convective, grid-scale, and total precipitation rates for S_a = −20, −30 and −40 mb. Compared with Figs. 2 and 4, noticeable differences are observed. In the experiment with S_a = −20 mb, the convective precipitation starts at 16 h and stops around 110 h, although very small amount of the convective precipitation is seen at certain times after 110 h. On the other hand, the convective precipitation in the case of S_a = −40 mb persists during the 8-day period and further time integration reveals that it stops at 239

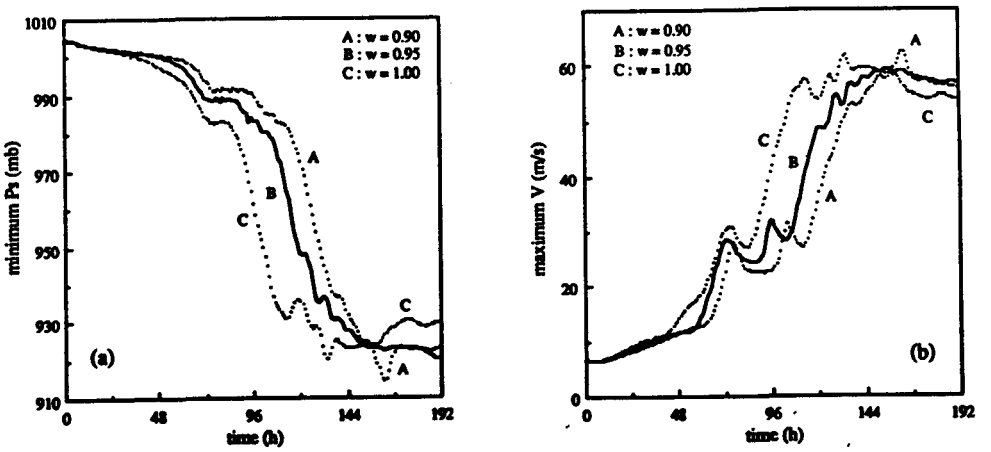

FIG. 3. Same as Fig. 1 except for the sensitivity experiments with different stability weights on the moist adiabat in the lower atmosphere.

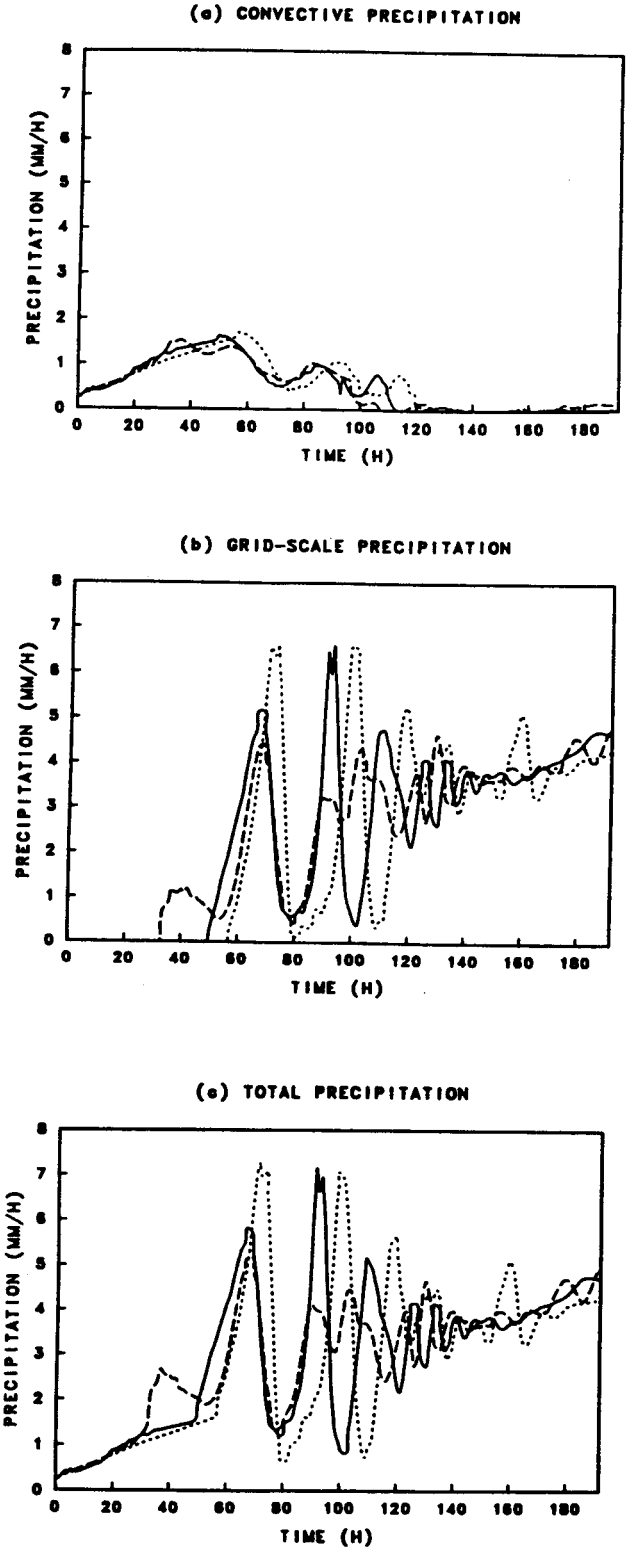

FIG. 4. (a) The time evolution of the inner 500 km domain-averaged convective, (b) grid-scale, and (c) total precipitation rates for the sensitivity experiments with different stability weights on the moist adiabat in the lower atmosphere. The dotted, solid, and dashed lines correspond to $w = 0.90$, 0.95 and 1.00, respectively.

h (not shown here). The convective precipitation rate with $S_a = -20$ mb is small compared with the other two storms. Figure 7b shows that the grid-scale precipitation with $S_a = -40$ mb begins at 110 h and the large amplitude oscillation in the time history of the grid-scale precipitation rate continues until the end of the time integration in the simulation with $S_a = -20$ mb. After 110 h, the period of this oscillation is about 15 h, which was also observed in the time evolution of the minimum surface pressure and maximum low level tangential wind speed (Fig. 5). Figures 5–7 show that variations in S_a have a significant impact on the behavior of model storm evolution. This indicates that this parameter should be chosen carefully when the Betts parameterization is used.

Figures 2, 4 and 7 show large oscillations in the grid-scale precipitation. As described in Part I, these appear to be related to the assumption that all of the liquid water that results from supersaturation evaporates into the next lower model layer. This causes the grid-scale latent heating profile to have a maximum at low levels and results in a rather rapid onset of grid-scale precipitation (when the lowest model level becomes saturated). In all of the sensitivity studies, the magnitude of this oscillation is increased when parameters are varied in such a way that the convective-scale heating decreases (increasing τ and decreasing the magnitude of S_a).

4. Sensitivity to the physical environment, initial conditions, and horizontal resolution

In this section, the sensitivity of the model to variations in the sea surface temperature, latitude, initial vortex structure, initial moisture distribution, and radiation is investigated. Also, experiments with various model horizontal resolutions are presented to study the effect of resolution on the partition between grid-scale heating and subgrid-scale heating as well as on the model storm evolution.

a. Sea surface temperature

Numerous studies (e.g., Ooyama 1969) have shown that the evolution of tropical cyclone is quite sensitive to variations in sea surface temperature. The energy that feeds the storm comes from the ocean primarily in the form of water vapor. Saturation water vapor pressure is exponentially related to temperature. So, when the sea surface temperature increases, there is a rapid increase of the surface saturation mixing ratio, and hence the amount of water vapor extracted from the ocean.

Figure 8 shows the time evolution of the minimum surface pressure, the maximum low level tangential wind speed, and the radius of 15 m s^{-1} tangential wind speed at level 15 for sea surface temperatures of 27°, 28° and 29°C. In this paper, the radius of the 15

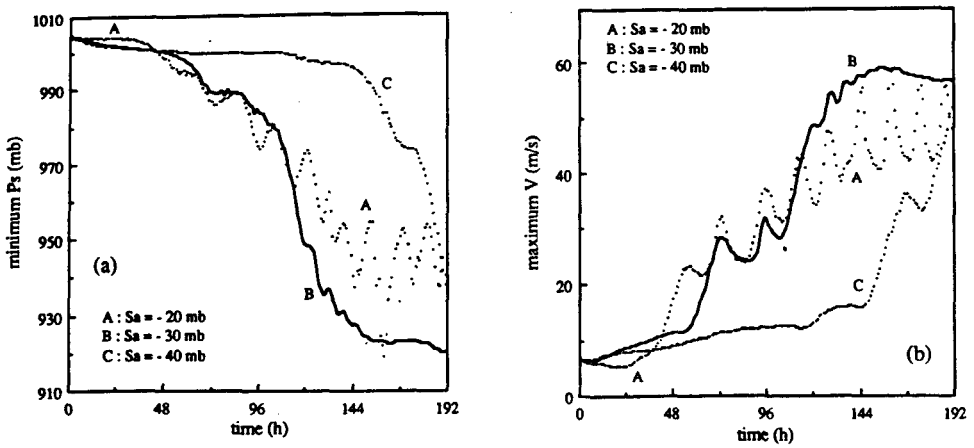

FIG. 5. As in Fig. 1 except for the sensitivity experiments with different saturation pressure departures at the lowermost model integer level.

m s^{-1} wind speed is selected to measure a storm size. As the sea surface temperature increases, the storm undergoes more rapid development and has a lower central pressure at the mature stage. Also, the storm size increases as the sea surface temperature increases. The storm size for the 27°C sea surface temperature changes little with time after around 96 h, while the storm sizes for the 28° and 29°C sea surface temperatures, generally speaking, continue to increase until the end of the time integration.

Emanuel (1988) has shown that the maximum intensity of hurricanes is controlled by the sea surface temperature and the average temperature in the layer in which the outflow occurs. In Part I, it was shown that the outflow in the control simulation occurs in a narrow layer between the $\sigma = 0.05$ and $\sigma = 0.15$. The ambient temperature within the outflow layer ranges from about −60° to −80°C. The minimum model surface pressures in Fig. 8a are about 940, 920 and 890 mb for sea surface temperatures of 27°, 28° and 29°C. Assuming an ambient surface relative humidity of 80% and outflow temperatures ranging from −60° to −80°C, the minimum possible surface pressures range from 945–910, 935–900 and 930–885 mb, for sea surface temperatures of 27°, 28° and 29°C, respectively (from Fig. 4a in Emanuel 1988). The model minimum surface pressures are within the range of estimates from Emanuel (1988), which indicates that the model produces a vortex which is close to its maximum possible intensity.

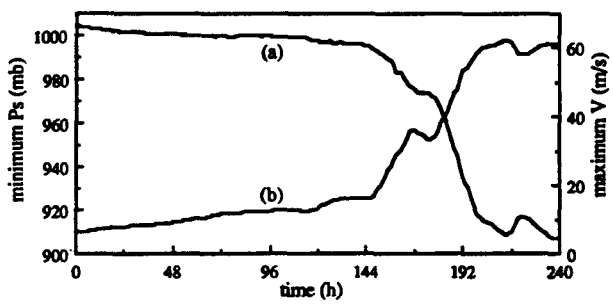

FIG. 6. (a) The time evolution of the minimum surface pressure, and (b) the maximum low level tangential wind speed for $S_a = -40$ mb during a 10-day time integration.

b. *Latitude*

The sensitivity of model storm evolution to latitude has been studied by many authors (e.g., Yamasaki 1968). Figure 9 displays the time evolution of the minimum surface pressure, the maximum low level tangential wind speed, and the radius of 15 m s^{-1} wind speed for latitudes of 10°, 20° and 30°N. The 8-day time integration was not enough to obtain a mature storm for the case of 30°N, so a 12-day simulation was performed (Fig. 10). It is shown that high-latitude storms intensify more slowly, but the intensity of the mature storm does not indicate any significant difference with latitude. Compared with the storms at 10° and 20°N, the storm at 30°N requires a considerably longer time period to develop. The time history of the radius of 15 m s^{-1} wind speed for the storm at 30°N (Fig. 10c) shows a gradual increase after around 168 h and the storm size near 288 h is slightly larger than that of the control case at the mature stage. Although the pattern of the time history of the radius of 15 m s^{-1} wind speed for the storm at 30°N is somewhat different from that of the storm at 10°N (or 20°N) because of the slower development, the model result supports previous studies (e.g., DeMaria and Pickle 1988) that suggest low-latitude storms are smaller than high-latitude storms.

c. *Initial vortex structure*

The initial vortex structure has an important influence on the subsequent evolution of model storm (e.g.,

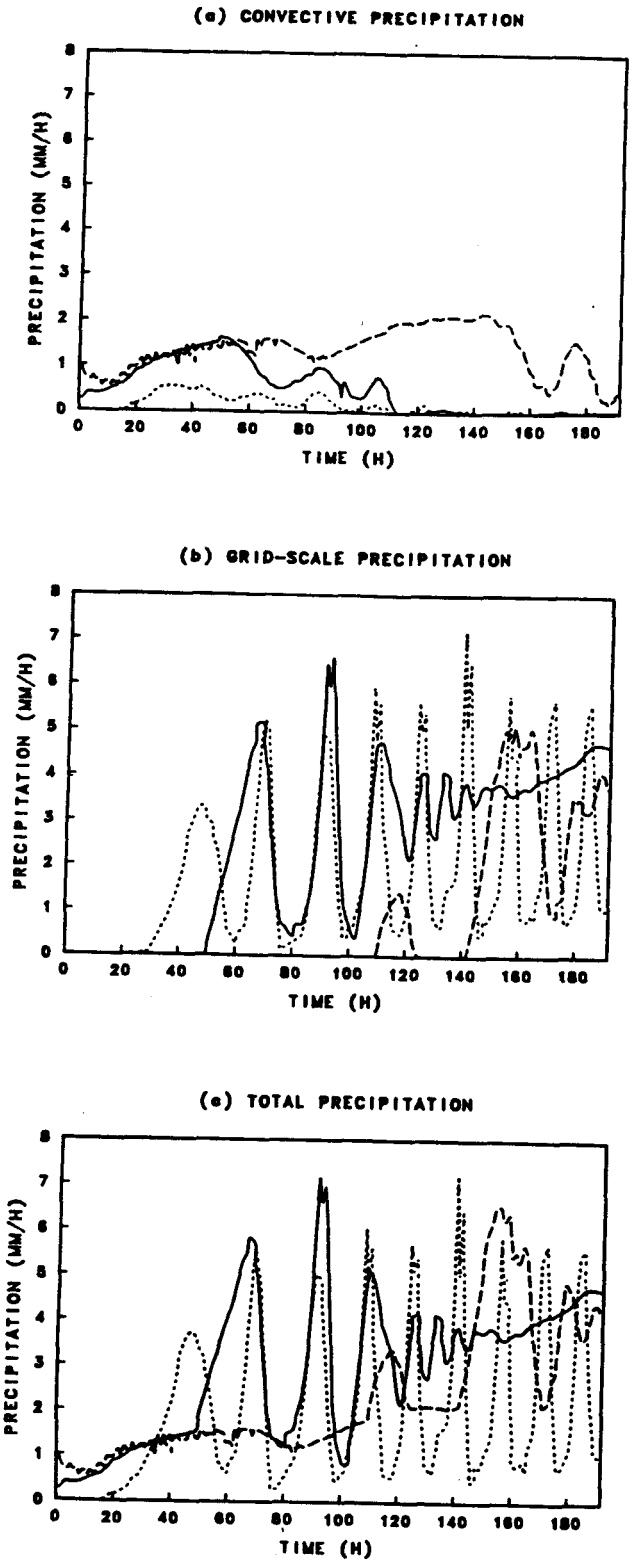

FIG. 7. (a) The time evolution of the inner 500 km domain-averaged convective, (b) grid-scale, and (c) total precipitation rates for the sensitivity experiments with different saturation pressure departures at the lowermost model integer level. The dotted, solid, and dashed lines correspond to $S_a = -20$, -30 and -40 mb, respectively.

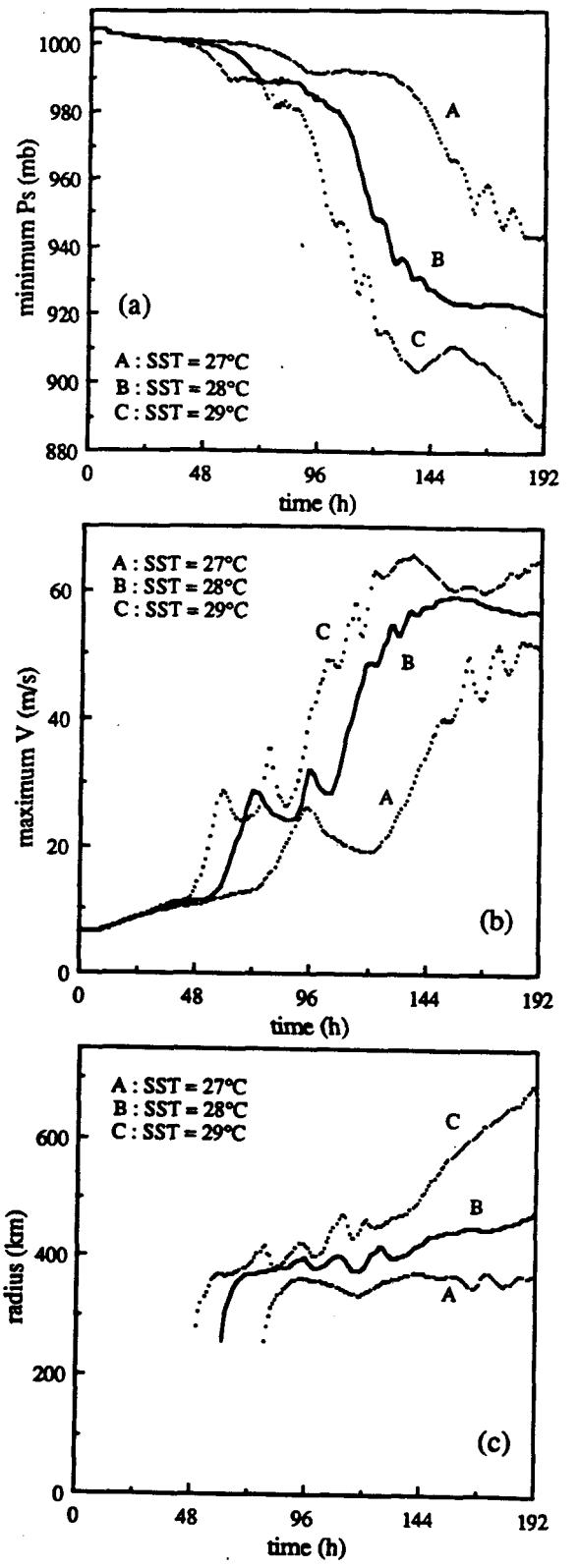

FIG. 8. (a) The time evolution of the minimum surface pressure, (b) the maximum low level tangential wind speed, and (c) the radius of 15 m s^{-1} tangential wind speed at level 15 for the sensitivity experiments to sea surface temperatures of 27°, 28° and 29°C.

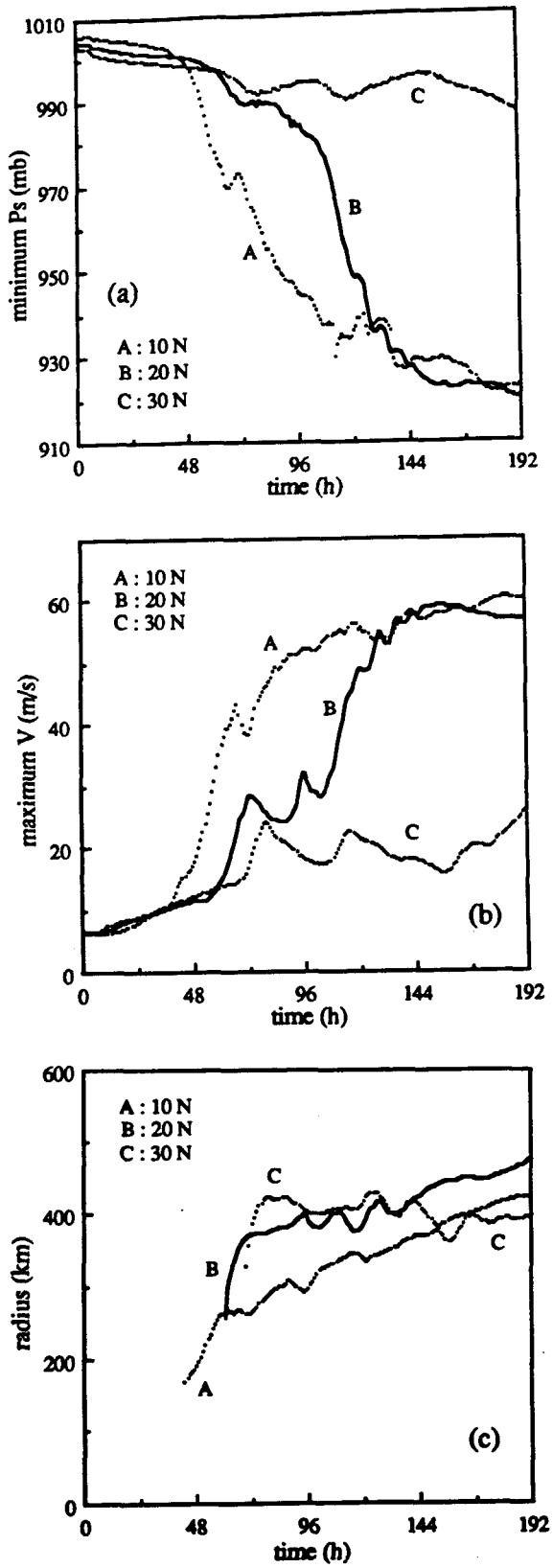

FIG. 9. As in Fig. 8 except for the sensitivity experiments to latitudes of 10°, 20° and 30°N.

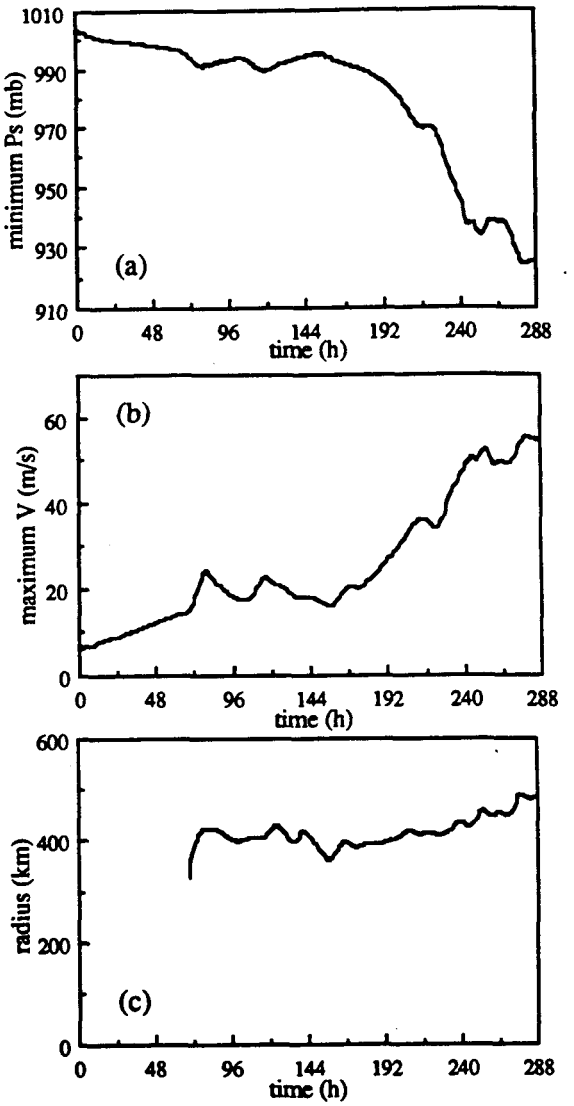

FIG. 10. (a) The time evolution of the minimum surface pressure, (b) the maximum low level tangential wind speed, and (c) the radius of 15 m s^{-1} tangential wind speed at level 15 for the case of 30°N during a 12-day time integration.

Rotunno and Emanuel 1987). To study this effect, simulations with different values of v_m, but the same values of r_m and σ_m (where v_m is the maximum tangential wind, r_m the radius of maximum wind, and σ_m the σ level of maximum wind) as the control run [see (2.11) in Part I] are carried out. Figure 11 shows the time evolution of the minimum surface pressure, the maximum low level tangential wind speed, and the radius of 15 m s^{-1} wind speed for $v_m = 3.5$ (half of the control run), 7 and 14 m s^{-1} (double of the control run). This figure indicates that the storm evolution is very sensitive to the initial vortex amplitude. The storm intensifies more rapidly and is larger as the initial vortex amplitude increases. Also, as the initial vortex ampli-

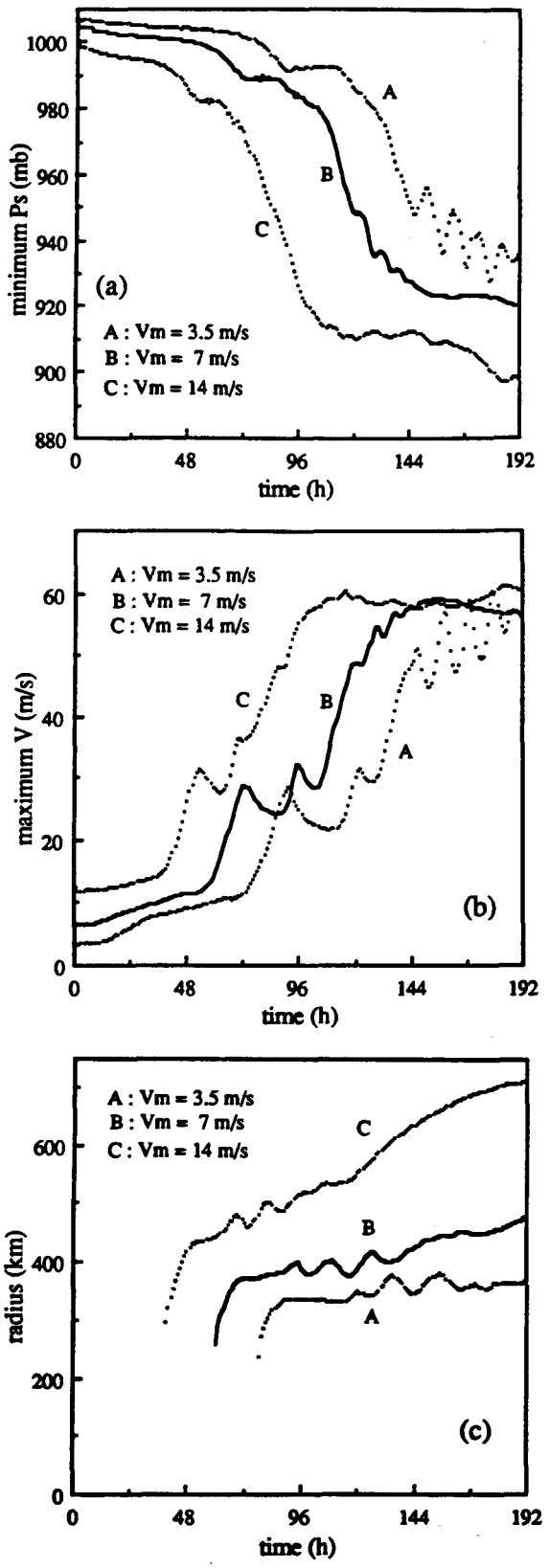

FIG. 11. As in Fig. 8 except for the sensitivity experiments to initial vortex amplitudes of 3.5, 7 and 14 m s^{-1}.

tude increases, the storm is more intense at the mature stage although the differences in final intensities are less pronounced in terms of the maximum wind speeds (Fig. 11b) compared with the minimum surface pressure (Fig. 11a). This is consistent with the fact that storms with the larger initial vortex amplitudes are larger (in terms of radius of 15 m s^{-1} winds) at the mature stage.

The effect of the initial vortex amplitude on the storm evolution can be understood in several ways. The initialization procedure described in section 2f of Part I yields a lower central pressure and a warmer state in the middle and upper troposphere near the model center as the initial vortex amplitude increases. The initial minimum surface pressures and maximum temperature deviations from the model lateral boundary for v_m = 3.5, 7, 14 m s^{-1} are 1007.1, 1004.9, 999.0 mb and 0.3°, 0.7°, 2.0°C, respectively. The energy supply from the ocean becomes large as the vortex amplitude increases, because the latent heat flux increases as the surface wind increases and as the surface pressure decreases. The inertial stability near the storm center also increases as the vortex amplitude increases. The efficiency at which heating increases the tangential wind speed and hence accelerates the storm development is larger in regions which are more inertially stable even if the diabatic heating rate is the same (Schubert and Hack 1982). Also, as the vortex amplitude increases, the relative vorticity in the lower troposphere increases, so the boundary layer pumping is enhanced because the frictionally induced vertical velocity at the top of the Ekman layer is proportional to the relative vorticity of the surface wind (Charney and Eliassen 1964).

Emanuel (1986) has suggested that tropical cyclone development is a consequence of a finite-amplitude instability. This was supported by the model results of Rotunno and Emanuel (1987) which showed that a tropical cyclone did not develop when the initial vortex amplitude was reduced from 12 to 2 m s^{-1}. In Fig. 11, it can be seen that the vortex with v_m = 3.5 m s^{-1} eventually develops. Additional simulations were performed with v_m = 2.0 and 1.0 m s^{-1} and development still eventually occurred. In the model results of Rotunno and Emanuel (1987), the initial thermodynamic structure was adjusted so that it was neutral to the model simulations. There is a small amount of convective instability in the initial condition used here, which may account for the development with a weak initial vortex. As described in the section 4d, the initial instability was reduced by adjusting the initial moisture distribution. In this case, the model storm did not develop with a weak initial vortex.

d. Initial moisture distribution

It is well known that high moisture content in the lower and middle troposphere is favorable for storm development (e.g., Rosenthal 1970). High moisture

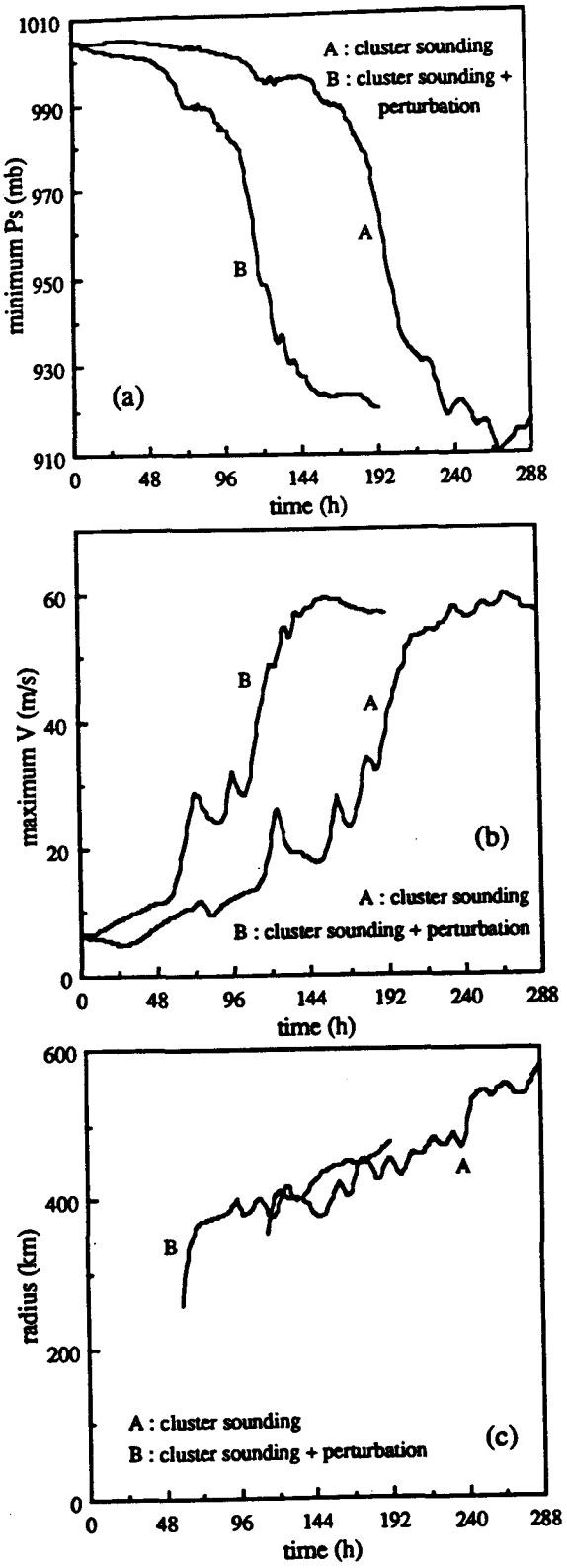

FIG. 12. As in Fig. 8 except for the sensitivity experiments to initial moisture distributions of the mean tropical cluster environment sounding and the mean tropical cluster environment sounding plus a Gaussian perturbation with the amplitude of 10% in relative humidity near the disturbance.

content in low and middle levels initially leads to high convective instability and therefore storm development is accelerated. In the control case, the initial relative humidity field consists of the mean tropical cluster environment sounding and a Gaussian type perturbation with a maximum amplitude of 10% near the disturbance center. Therefore, the initial relative humidity field is a function of radius (r) and height (σ). To investigate the effect of initial moisture distribution on the storm evolution, an experiment is conducted in which only the mean tropical cluster environment sounding for initial moisture distribution is used, so the initial relative humidity field is a function of height only. For this case, the model was integrated up to 12 days.

Figure 12 displays the time evolution of the minimum surface pressure, the maximum low level tangential wind speed, and the radius of 15 m s^{-1} wind speed for the cluster sounding (A) and the cluster sounding plus the perturbation (B) cases. As should be expected, the initial high moisture content near the disturbance (B) causes considerably earlier development of the storm. At the mature stage, storm A exhibits a slightly lower central pressure than storm B (Fig. 12a), but the maximum low level tangential wind speeds are about the same (Fig. 12b). Both storms show a gradual increase in the radius of 15 m s^{-1} wind speed during the time integration.

The simulation without the moisture perturbation was repeated with v_m = 2 m s^{-1}. In this simulation, the model storm did not develop, consistent with the results of Rotunno and Emanuel (1987).

e. Radiation

The magnitude of diabatic heating or cooling associated with radiative processes is small compared with that of diabatic heating due to cumulus convection during nearly the entire lifetime of a tropical cyclone. However, as mentioned in Part I, there are several numerical studies (e.g., Sundqvist 1970) that show that differential radiative cooling during the early stage accelerates storm development by enhancing baroclinicity and driving radial-vertial flows. Figure 13 shows the time evolution of the minimum surface pressure, the maximum low level tangential wind speed, and the radius of 15 m s^{-1} wind speed with and without the radiation physics. The storm with the net radiational cooling effect exhibits slightly earlier development than the storm without it, but the radiational cooling has little influence on the storm intensity and size at the mature stage. After about 120 h, the storm without the radiational cooling shows some oscillations in the time history of the minimum surface pressure and the maximum low level tangential wind speed.

In the present paper, only net radiational cooling is included. However, there is some observational evidence (e.g., Zehr 1987) that tropical cyclones experience diurnal variations. Further study using a numer-

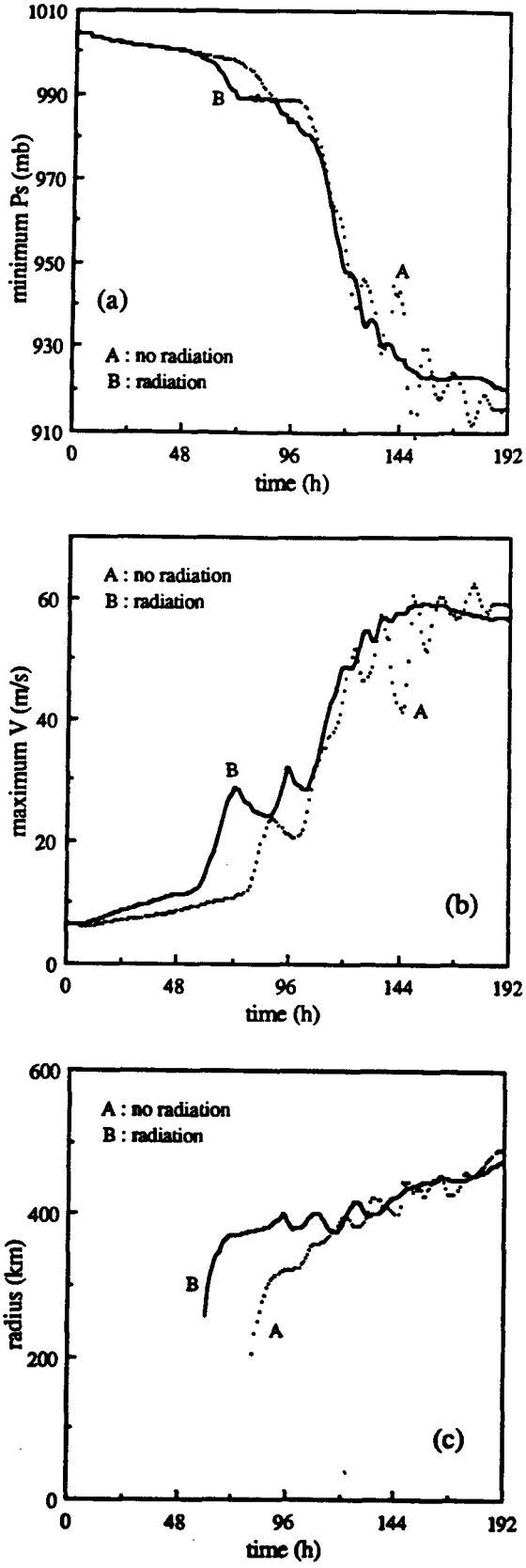

FIG. 13. As in Fig. 8 except for the sensitivity experiments to radiation for cases with and without the net radiational cooling effect.

ical model with shortwave and longwave radiation parameterizations is needed to investigate diurnal variations of tropical cyclones.

f. Horizontal resolution

Figure 2 in Part I showed that the partition of the latent heating between grid-scale and subgrid-scale effects varied considerably during the model simulation. To investigate how this partition is affected by the model resolution, simulations with horizontal resolutions of 40 and 60 km are performed. Figure 14 displays the time evolution of the minimum surface pressure, the maximum low level tangential wind speed, and the radius of 15 m s^{-1} wind speed for horizontal resolutions of 20, 40 and 60 km. In the case of 60 km resolution, the storm does not develop. The magnitude of the subgrid-scale heating produced by the convective adjustment scheme is too small for the initial vortex to grow. Compared with the 20 km case, the 40 km case shows much slower storm development. The storm with 40 km resolution did not reach a mature stage at the end of 12 days. These results show that there is an upper limit of horizontal resolution beyond which the model cannot simulate the essential features of a tropical cyclone. The upper limit is believed to be dependent on the cumulus parameterization scheme as well as other model physics, the physical environment, and the initial conditions. Anthes (1977b) showed that it was possible to simulate a tropical cyclone in an axisymmetric model with a 60 km horizontal resolution which used a modified Kuo parameterization scheme (Anthes 1977a). This suggests that it may be more difficult to simulate tropical cyclones with the Betts scheme, compared with the Kuo scheme. However, a more careful comparison would be necessary to confirm this result.

Figure 15 shows the time evolution of the inner 500 km domain-averaged total, grid-scale, and convective precipitation rates for the horizontal resolution of 40 km. Compared with the 20 km case (Fig. 2 in Part I), the 40 km case shows a higher convective precipitation rate and the convective precipitation continues for the entire time integration period. As might be expected, the subgrid-scale heating becomes a larger fraction of the total heating as the horizontal grid size is increased.

The reduced development with the 40 km resolution and the lack of development with the 60 km resolution suggest that it may not be possible to simulate the mature stage of a tropical cyclone with the Betts scheme (with the convective adjustment parameters as in the control run), but without the grid-scale heating. This is supported by the sensitivity to the parameter S_a as was shown in Figs. 5–7. When the magnitude of S_a was increased to −40 mb, the onset of the grid-scale heating was delayed, as was the period of rapid intensification. Thus, in a model with relatively coarse resolution (such as a global model) where the grid-scale

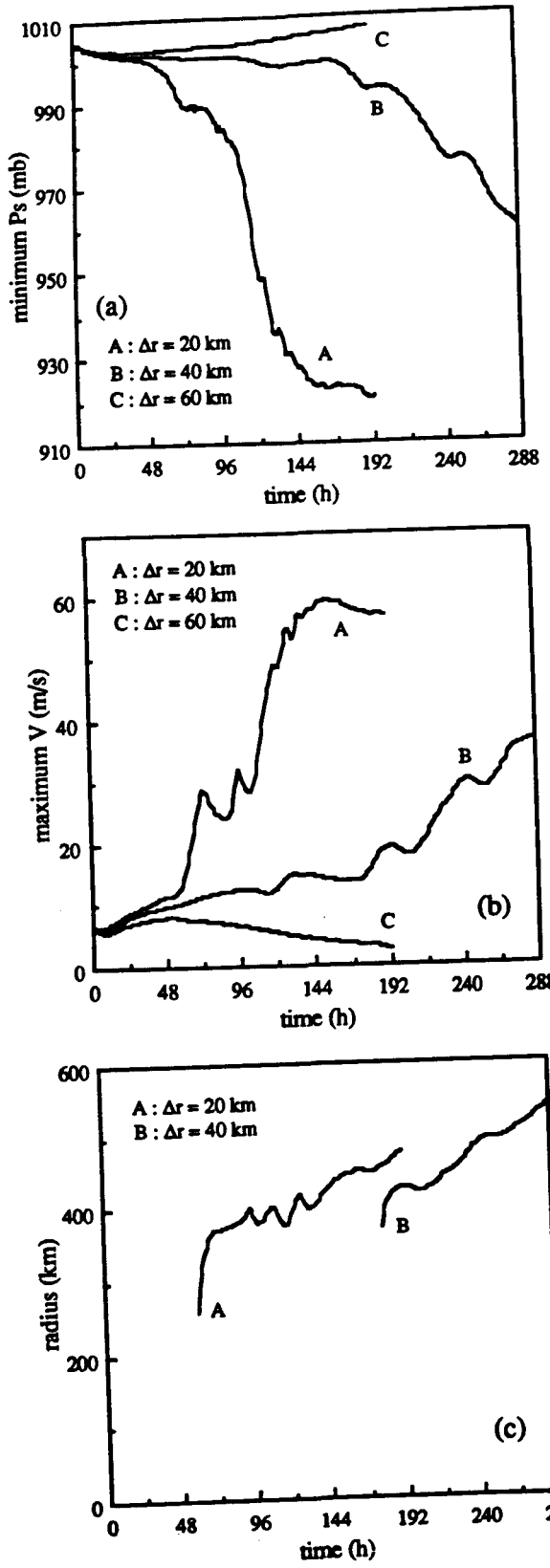

FIG. 14. As in Fig. 8 except for the sensitivity experiments to horizontal model resolutions of 20, 40 and 60 km.

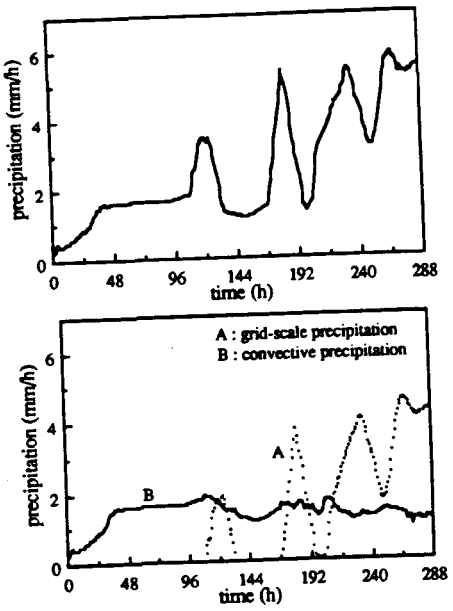

FIG. 15. The time evolution of the inner 500 km domain-averaged total precipitation rate (upper panel) and grid-scale and convective precipitation rates (lower panel) for the horizontal resolution of 40 km.

heating is greatly reduced, the use of the Betts scheme may lead to decreased tropical cyclone activity.

The results of the sensitivity experiments summarized in this section are similar to previous other studies. All cases discussed thus far, except for the 60 km resolution case, could simulate the tropical cyclone development. Further research is required to determine necessary conditions for the Betts scheme to simulate nondevelopment and to simulate development without grid-scale heating.

5. Summary and conclusions

In this paper, extensive sensitivity experiments were performed with the axisymmetric tropical cyclone model described in Part I, which includes the moist convective adjustment scheme described by Betts (1986). The sensitivity of the model storm evolution to the adjustment parameters was examined to further understand the convective parameterization scheme. Numerical simulations showed that as the adjustment time scale is decreased and the stability weight on the moist adiabat in the lower atmosphere is increased, the time period before the storm develops is reduced. The model storm evolution is quite sensitive to variations in the saturation pressure departure at the lowermost model integer level and the mature storm attains a lower minimum surface pressure as the magnitude of the saturation pressure departure becomes large. Variations in the adjustment parameters have influences on the grid-scale precipitation as well as the convective precipitation. The precipitation is particularly sensitive to changes in the saturation pressure departure.

The sensitivity of the storm evolution to the physical environment, initial conditions, and model horizontal resolution was also studied. The results from the sensitivity experiments to sea surface temperature, latitude, initial vortex amplitude, initial moisture distribution, and radiation are similar to previous studies. When the horizontal grid size was increased from 20 to 60 km, the storm did not develop. A storm did develop with 40 km resolution although it was less intense than the 20 km case. For the 40 km resolution, the subgrid-scale heating was a larger fraction of the total heating compared with the case with 20 km resolution. These results suggest that it may not be possible to simulate tropical cyclone development with the Betts scheme, but without grid-scale heating unless the convective adjustment parameters are modified.

Compared with other cumulus parameterization schemes (Kuo 1965, 1974; Arakawa and Schubert 1974), the Betts convective parameterization scheme sidesteps the details of how the subgrid-scale cumulus clouds interact with the large-scale environment. This might be considered a disadvantage of the scheme. However, the convective adjustment scheme is simple and can give more realistic heating and moistening in the vertical due to cumulus convection because the construction of the reference profiles is based on observations. Another advantage is that it includes shallow convection as well as deep convection. The current version of the convective scheme constructs the reference profiles using only thermodynamic considerations. An interesting extension of this work would be to include the effect of wind shear in the scheme to simulate convection in baroclinic regions.

Acknowledgments. The authors would like to thank James Hack and Alan Betts for providing valuable comments on this study. This research was supported by National Science Foundation under Grants ATM-8521611 and ATM-8817763. Part of the computer time for this research was provided by the Naval Research Laboratory.

REFERENCES

Anthes, R. A., 1977a: A cumulus parameterization scheme utilizing a one-dimensional cloud model. *Mon. Wea. Rev.*, **105**, 270–286.

——, 1977b: Hurricane model experiments with a new cumulus parameterization scheme. *Mon. Wea. Rev.*, **105**, 287–300.

Arakawa, A., and W. H. Schubert, 1974: Interaction of a cumulus cloud ensemble with the large-scale environment, Part I. *J. Atmos. Sci.*, **31**, 674–701.

Baik, J.-J., M. DeMaria and S. Raman, 1990: Tropical cyclone simulations with the Betts convective adjustment scheme. Part I: Model description and control simulation. *Mon. Wea. Rev.*, **118**, 513–528.

Betts, A. K., 1986: A new convective adjustment scheme. Part I: Observational and theoretical basis. *Quart. J. Roy. Meteor. Soc.*, **112**, 677–691.

——, and M. J. Miller, 1986: A new convective adjustment scheme. Part II: Single column tests using GATE wave, BOMEX, ATEX and arctic air-mass data sets. *Quart. J. Roy. Meteor. Soc.*, **112**, 693–709.

Charney, J. G., and A. Eliassen, 1964: On the growth of the hurricane depression. *J. Atmos. Sci.*, **21**, 68–75.

DeMaria, M., and J. D. Pickle, 1988: A simplified system of equations for simulation of tropical cyclones. *J. Atmos. Sci.*, **45**, 1542–1554.

Emanuel, K. A., 1986: An air–sea interaction theory for tropical cyclones. Part I: Steady-state maintenance. *J. Atmos. Sci.*, **43**, 585–604.

——, 1988: The maximum intensity of hurricanes. *J. Atmos. Sci.*, **45**, 1143–1155.

Kuo, H. L., 1965: On formation and intensification of tropical cyclones through latent heat release by cumulus convection. *J. Atmos. Sci.*, **22**, 40–63.

——, 1974: Further studies of the parameterization of the influence of cumulus convection on large-scale flow. *J. Atmos. Sci.*, **31**, 1232–1240.

Ooyama, K. V., 1969: Numerical simulation of the life cycles of tropical cyclones. *J. Atmos. Sci.*, **26**, 3–40.

Rosenthal, S. L., 1970: A circularly symmetric primitive equation model of tropical cyclone development containing an explicit water vapor cycle. *Mon. Wea. Rev.*, **98**, 643–663.

Rotunno, R., and K. A. Emanuel, 1987: An air–sea interaction theory for tropical cyclones. Part II: Evolutionary study using a nonhydrostatic axisymmetric numerical model. *J. Atmos. Sci.*, **44**, 542–561.

Schubert, W. H., and J. J. Hack, 1982: Inertial stability and tropical cyclone development. *J. Atmos. Sci.*, **39**, 1687–1697.

Sundqvist, H., 1970: Numerical simulation of the development of tropical cyclones with a ten-level model. Part II. *Tellus*, **22**, 504–510.

Yamasaki, M., 1968: Numerical simulation of tropical cyclone development with the use of primitive equations. *J. Meteor. Soc. Japan*, **46**, 202–214.

Zehr, R. M., 1987: The diurnal variation of deep convective clouds and cirrus with tropical cyclones. *17th Conference on Hurricanes and Tropical Meteorology*, Miami, Amer. Meteor. Soc., 276–279.